Functional Assessment for Predicting Charge-Transfer Excitations of Dyes in Complexed State: a Study of Triphenylamine-Donor Dyes on Titania for Dye-Sensitized Solar Cell

Pratibha Dev,*,† Saurabh Agrawal,†,‡ and Niall J. English†

SEC Strategic Cluster, School of Chemical and Bioprocess Engineering, University College Dublin, Belfield, Dublin 4, Ireland

E-mail: pratibha.dev@ucd.ie

Keywords: Excited States, Quantum Chemistry, TD-DFT, Photo-physics, ab-initio

Abstract

Time-dependent density functional theory (TD-DFT) was employed to calculate the UV/Vis spectra for three of the triphenylamine (TPA)-donor dyes – TC1, L1 and LJ1 – in isolation as well as when complexed with a titania nanoparticle. TPA-donor dyes are a class of promising organic dyes for the use in dye-sensitized solar cells (DSSCs). The three dyes studied here are amongst the smallest of these dyes and provide important insight into the entire series of TPA dyes that are being explored as possible sensitizers in titania-based DSSCs. An attempt to calculate the optical spectra for these dyes within the B3LYP approximation to the exchange

*To whom correspondence should be addressed

†SEC Strategic Cluster, School of Chemical and Bioprocess Engineering, University College Dublin, Belfield, Dublin 4, Ireland

‡Istituto CNR di Scienze e Tecnologie Molecolari c/o Dipartimento di Chimica, Università di Perugia, via Elce di Sotto 8, I-06123, Perugia, Italy

correlation functional produces erroneous results. On the other hand, Coulomb Attenuated Approximation (CAM-B3LYP) captures the correct photo-physics of the dyes and produces more accurate charge-transfer excitation energies of their complexes with titania. This work shows that the extent to which a given approximation fails or succeeds to correctly predict the charge-transfer excitation energies in the isolated dyes is propagated in that it fails (or succeeds) to correctly predict the values of the excitation energies for the complexes. It is, therefore, important to determine the most appropriate functional for a dye before considering it in more complicated structures such as dye-titania complexes.

Introduction

There is a considerable research interest in developing and improving alternative energy devices such as solar cells. Conventional solar cells are mostly silicon-based devices. On the other hand, dye-sensitized solar cells (DSSCs) as proposed by Grätzel et al.[1] represent a new paradigm in harvesting solar energy. This possibility of creating a new type of solar cell has resulted in a large amount of experimental and theoretical work across disciplinary boundaries in search of stable and efficient DSSCs. Typically, a DSSC consists of two electrodes that sandwich the active components – a metal-oxide semiconductor functionalized by appropriate dye (dyes) and an I^-/I_3^--based electrolyte.[2] The overall efficiency of DSSCs depends upon the dye(s) employed in the cell, the nature of metal oxide film as well as on an details of charge transfer and charge transport processes in the cell.[3,4]

At the heart of a DSSC is the dye adsorbed onto the metal-oxide semiconductor (mostly, a nanocrystalline film of titania, TiO_2). Unmodified titania absorbs only in UV range (optical bandgap of the bulk anatase titania $\sim 3.2\,eV$[5]) and needs to be functionalized with an appropriate dye that introduces additional states within the bandgap. This allows the cell to absorb light in the visible range of the spectrum. Ideally, one wants a dye that has a wide absorption spectrum, thereby, improving the overall efficiency of the cell. So far, ruthenium-based sensitizers are one of the best dyes that give the highest-energy conversion efficiencies exceeding 11%.[6–8] However, the

presence of ruthenium in these dyes increases their cost considerably. Hence, various organic dyes are now being investigated as alternatives to the ruthenium-based dyes. These organic dyes are advantageous due to several reasons: (a) their lower cost, and (b) ease with which small structural modifications change their photo-physical and electrochemical properties.[9,10]

An organic dye for DSSCs usually consists of an electron-donating group (donor), a spacer or a linker moiety and an electron-accepting group (acceptor) that also anchors the dye to the titania surface. This particular structure – donor group linked to the acceptor group through an appropriate spacer/linker group – provides the desirable pull-push effect that is needed for efficient charge separation in dyes for DSSCs. A lot of experimental effort has been dedicated to creating better, more stable dyes. To this end, numerous dyes with different donors, linkers and acceptors have been synthesized and their performance as photo-sensitizers evaluated experimentally (see, for example, review articles by Mishra *et al*[9] and Hagfeldt *et al*[4]). On the theoretical side, numerous studies[11–23] have been carried out to understand the photo-physics of dyes by themselves and in complexes with titania thin-films or nanoparticles. Most of these studies utilize time-dependent density functional theory (TD-DFT) to calculate UV/Vis spectra of the systems of interest.

TD-DFT provides a computationally inexpensive tool to study the electronic excitations of matter in presence of time-dependent perturbations. Although, TD-DFT is formally an exact theory, it relies on adiabatic approximation. This approximation neglects the temporal non-locality (memory effects) and assumes that at any given moment, the exchange-correlation (*xc*) functional depends only on the instantaneous density. In turn, this allows the use of traditional (time-independent) approximations to the *xc*-functional derived for ground state DFT, such as generalized gradient approximation, GGA (for example, GGA of Perdew, Burke and Ernzerhof, PBE[24]) and hybrid functionals containing a fixed percentage of exact exchange (for example, B3LYP[25–27]). The choice of approximations to the *xc*-functional critically decides the accuracy of the TD-DFT results in the case of charge transfer (CT) excitations. For example, the exchange-correlation potentials generated from local and semilocal functionals (for example, PBE) decay too rapidly. They do not contain the correct $1/R$-asymptotic behavior, where R is the distance between charges. As a result,

TD-DFT within these local/semilocal approximations is mostly unable to describe the transitions involving substantial intramolecular/intermolecular charge transfer.[28,29] One way to alleviate the aforementioned problem is by including a fixed percentage of Hartree-Fock exchange in the *xc*-functional. These hybrid functionals, such as B3LYP that contains the (0.2)/*R*-dependence, offer some improvement in describing the CT excitations. However, even the conventional hybrid functionals do not work for all systems.[30]

Another class of functionals – range-separated exchange-correlation functionals – provides an alternative to the local/semi-local and conventional hybrid functionals. From amongst these long-range corrected functionals, we have chosen to study the excited state properties using CAM-B3LYP.[31] Within CAM-B3LYP, the exchange term is split into short- and long-range components. The short-range component is dominated by DFT exchange and contains only 19% exact exchange. On the other hand, the percentage of Hartree-Fock exchange increases at larger distances and the functional contains upto 65% exact exchange in its long-range component. This improvement in the asymptotic behavior of the functional leads to better description of the CT interactions in many cases where B3LYP fails. However, it is not always the case and one needs to select the suitable functional depending on the details of system under consideration.[32]

The focus of this work is to study the excited state properties of dye-titania complexes. Such studies are important as they shed light on the relationships between structural (and hence, electronic) properties of dyes, their complexes with titania and their performance within the solar cells. Therefore, it is important to understand how the choice of a functional affects the accuracy of TD-DFT results. As charge transfer excitations are important to this research, we have concentrated on the conventional hybrid functionals and on the range-separated functionals only. In the present work, UV/VIS spectra are calculated using time-dependent density functional theory (TD-DFT) within two approximations to *xc*-functional – B3LYP and CAM-B3LYP. Here we have considered three triphenylamine (TPA)-donor dyes – TC1, L1 and LJ1 dyes.[30,33,34] These dyes were chosen for two reasons: (1) their derivatives are promising dyes for the use in DSSCs,[30,33–36] and (2) it is harder to capture the right photo-physics of most of the TPA-dyes using local, semi-local or

even conventional hybrid functionals.[23] In this sense, they provide a unique opportunity to test the robustness of TD-DFT results using various approximations to *xc*-functional. It is shown that in order to get the electronic excitation energies of the isolated TPA-dyes correctly, one needs to use Coulomb Attenuated Approximation (CAM-B3LYP), while the usual hybrid functional, B3LYP gives less accurate description of the intramolecular charge-transfer excitations in the dyes. The functional performance for the three dyes can be correlated to the extent of spatial overlap of the filled and virtual orbitals involved in the transition.[23,32,37–40] A dye-titania complex offers an even more complicated system and we have explored the limits of accuracy to which one can study such systems within TD-DFT. Even though CAM-B3LYP substantially overestimates the optical bandgap of the titania nanoparticle as compared to the B3LYP approximation, the use of CAM-B3LYP approximation gives far more accurate results for the complex as compared to B3LYP.

Although, we have studied only three different complexes here, this study provides a simple guideline that may be used when predicting charge-transfer excitations in composite structures in which only one component is photoactive in the spectral range of interest. It will be shown in this work that the extent to which a given approximation fails (or succeeds) to correctly predict the CT excitation energies for the isolated dyes within a given approximation is propagated in the extent it fails (or succeeds) to correctly predict the values of excitation energies for the complexes. These results are discussed in greater details within the subsequent sections. The rest of the paper is organized as follows: The second section gives the methodology and computational details. In the third section, we provide the results of our TD-DFT calculations for the isolated systems (dyes and titania nanoparticle) within different functionals and discuss their performance. In the fourth section, the work is extended to study the dye-titania complexes and we discuss our results. The last section is a summary of the results and their application in future works.

Calculation Details

Discovery Studio Visualizer package (Accelrys, San Diego, CA) was used to model TC1, L1 and LJ1 dyes. All of these organic dyes contain TPA as donor and cyanoacrylic acid as electron acceptor. The linker group varies between the three dyes, as can be seen in Figure 1(a)-(c). TC1 contains a single methine unit that links the donor to the acceptor. Within L1, the linker group is extended by the addition of a thiophene unit, lengthening the π-conjugated system. In LJ1, there is a further improvement in the design of the dye through the replacement of thiophene unit by one of its electron-rich derivatives – 3,4-ethylenedioxythiophene (EDOT) unit. These structural modifications lead to an improvement in the efficiencies of the DSSCs based on these dyes from a mere 2.47% for TC1 [33] to 2.75% for L1 [30] and finally, to 7.30% for LJ1. [34]

We used Gaussian 09 software suite [41] to study the isolated dyes and dye-titania complexes. Here, we have tested the accuracy of two *xc*-functionals in describing the excitations in the TPA dyes: (a) Becke-3 Lee–Yang–Parr (B3LYP) hybrid functional and (b) the coulomb attenuated functional, CAM-B3LYP. We carried out all calculations using the standard 6-31G* basis set. In the first step of the calculations, we performed ground state structural optimization for the isolated dyes within respective functionals. After geometry optimization, we used TD-DFT to obtain the UV/VIS spectra of the three dyes. As theoretical results were compared to those obtained in the experiments, we added the effects of the respective solvents using the polarizable continuum model of solvation (C-PCM) [42] in all calculations. Use of continuum models ensures that important bulk solvent effects are included in the calculations. The solvents used in this study are: methanol for TC1 and acetonitrile for L1 as well as, for LJ1.

The next step in this work was to create dye-titania complexes and study their ground and excited state properties. For the complexes, we used a stoichiometric cluster of anatase titania [$(TiO_2)_{38}$], exposing its (101) surface. This nanoparticle geometry has been used and reported in earlier works [11,12,19,21,22] where it was shown that the lowest excitation energy of the $(TiO_2)_{38}$ cluster is in agreement with the experimental bandgap. We performed geometry optimization of the isolated titania cluster within the two functionals and used its ground state structure to create dye-

titania complexes. These conjugated structures were also subjected to geometry optimization to minimize the forces on the constituent atoms. Although, it is computationally very expensive, we carried out this step within Gaussian 09 software suite using 6-31G* basis set. A common practice for relaxing such a large system is to perform geometry optimization using one of the several plane-wave codes to make the calculations more manageable. Although, this practice results in a reasonable structure, the system is not in its ground state when such a relaxed structure is imported from a different code that had used a different basis set and/or pseudopotentials. In such cases, the structure should be re-optimized within the approximations and basis set that one proposes to use for calculating excited state properties. A failure to do so would mean that in the TD-DFT calculations, one is exciting a system that is not exactly in its ground state. In the last step, we carried out TD-DFT calculations to obtain the UV/Vis spectra for the dyes-titania complexes. Throughout the calculations, we maintained consistency by using the same level of theory and the basis set as that used for the isolated dyes.

Absorption Spectra of Isolated Systems

The experimental UV/Vis absorption spectra show maximum absorbance at energies of ~ 3.10 eV for TC1,[33] ~ 3.07 eV for L1[30,34] and ~ 2.91 eV for LJ1.[34] Figure 2 shows the UV/Vis spectra of the three isolated dyes as calculated within the B3LYP and CAM-B3LYP approximations. Table 1 and Table 2 summarize the TD-DFT results within the two approximations to the *xc*-functionals. Table 1 provides the singlet excitation energies at maximum absorbance, $\lambda_{max}^{Th.}$, the positions of HOMO, LUMO and the HL gaps ($\Delta_{HL} = \mathrm{E_{LUMO}} - \mathrm{E_{HOMO}}$) for the dyes. There are several important points to notice:

1. For the dyes studied here, the calculated values of the $\Delta_{HL} > \lambda_{max}^{Th.}$, showing the importance of correlation effects.[43]

2. The errors in the excitation energies calculated within CAM-B3LYP approximation are smaller than the B3LYP counterparts.

Table 1: Calculated wavelength at maximum absorbance ($\lambda_{max}^{Th.}$) and the corresponding HOMO (H), LUMO (L) positions and H-L gap ($\Delta_{HL} = E_{LUMO} - E_{HOMO}$) in eV. For titania, the table provides the value of the lowest transition (1^{st} Trans.), valence band maximum (VBM) and the conduction band minimum (CBM) as well as the bandgap (E_g).

System	Approx.	$\lambda_{max}^{Th.}$	H	L	Δ_{HL}
TC1	B3LYP	2.80	-5.50	-2.45	3.05
$\lambda_{max}^{Expt.}$=3.10[33]	CAM-B3LYP	3.28	-6.70	-1.28	5.42
L1	B3LYP	2.20	-5.21	-2.76	2.45
$\lambda_{max}^{Expt.}$=3.07[30,34]	CAM-B3LYP	2.94	-6.40	-1.63	4.77
LJ1	B3LYP	2.24	-5.14	-2.65	2.49
$\lambda_{max}^{Expt.}$=2.91[34]	CAM-B3LYP	2.88	-6.33	-1.55	4.78
	Approx.	1^{st} Trans.	VBM	CBM	E_g
TiO_2	B3LYP	3.80	-7.54	-3.02	4.52
	CAM-B3LYP	4.43	-9.22	-1.65	7.57

Table 2 gives the details of the transitions corresponding to $\lambda_{max}^{Th.}$ for the three dyes. In all cases, the largest percentage contribution (as deduced from the Configuration Interaction Singles coefficients) comes from the promotion from the highest occupied molecular orbital (HOMO) to the lowest unoccupied molecular orbitals (LUMO). Within the CAM-B3LYP approximations, there are also minor orbital pairs involved in the transitions. Figure 3(a)-(f) are the isosurface plots (isovalue = 0.02 e/a.u.^{3}) of the frontier orbitals for the TC1, L1 and LJ1 dyes. The HOMOs of the dyes are fairly delocalized over the respective molecules, though they show slightly more localization on the TPA-donor and spacer moieties than on the acceptor. On the other hand, the LUMOs are mostly localized on the acceptor (cyanoacrylic acid) and the spacer groups with negligible contribution from the donor group. This is highly desirable in the dyes synthesized for DSSCs as it leads to sufficient charge separation upon photo-excitation that in turn, reduces charge recombination. In going from TC1 to LJ1, there is an increase in the length of the π-conjugated system (spacer) via addition of the thiophene in L1 and the EDOT unit in LJ1. This results in a red shift seen in the L1 and the LJ1 spectra relative to the TC1 spectrum.

One can understand the functional performance through its correlation to the spatial overlap between the orbitals involved in the transition.[23,32] The small spatial overlap between the frontier orbitals [see, Figure 3(a)-(f)] of the TC1, L1 and LJ1 dyes means that there is a large rearrangement

Table 2: Details of transitions corresponding to $\lambda_{max}^{Th.}$ for the dyes. Abbreviations used: **T.E.** = Transition Energy (=$\lambda_{max}^{Th.}$), **O.S.** = Oscillator Strength, and **Coeff.** refers to the Configuration Interaction Singles coefficients (magnitude only).

Dyes Approx.	T. E. (eV) (O.S.)	Involved Orbitals (Coeff.)
TC1		
1) B3LYP	2.80 (0.94)	**H→L (0.70)**
2) CAM-B3LYP	3.28 (1.13)	**H→L (0.68)**, H-1→L (0.12)
L1		
1) B3LYP	2.20 (0.94)	**H→L (0.71)**
2) CAM-B3LYP	2.94 (1.21)	**H→L (0.64)**, H-1→L (0.26) H→L+1 (0.13)
LJ1		
1) B3LYP	2.24 (0.97)	**H→L (0.71)**
2) CAM-B3LYP	2.88 (1.20)	**H→L (0.64)**, H-1→L (0.25) H→L+1 (0.11)

of charge upon photoexcitation. Local/semi-local as well as, the conventional hybrid functionals fail to describe such CT transitions accurately. On the other hand, the long-range corrected functionals outperform the others in such cases. As can be seen in Figure 3(a)-(f), the overlap between HOMO-LUMO of TC1 is larger than that between the frontier orbitals of L1 or LJ1. This spatial overlap can also be quantified[32] through the inner product of the ground state occupied molecular orbital (MO), $\psi_i = \sum_\alpha C_{\alpha,i}\varphi_\alpha$ and virtual molecular orbital, $\psi_a = \sum_\beta C_{\beta,a}\varphi_\beta$. Here, the MOs have been written in the atomic-orbital (AO) basis set, $\{\varphi_\alpha\}$ and $C_{\alpha,i}$'s are the respective coefficients for the i^{th} MO.

Using the simpler definition used by Dev *et al.*,[23] one can write the orbital overlap as:

$$O_{ia} = \frac{\sum_\alpha (|C_{\alpha,i}|)(|C_{\alpha,a}|)}{\sum_\alpha (C_{\alpha,i})^2 \sum_\beta (C_{\beta,a})^2} \quad (1)$$

Without the absolute values of coefficients in Eq. 1, one will get a null result (to the numerical accuracy) for the various orbital pairs. For excitations involving several pairs of occupied-virtual states, the overlap measure as defined in Eq. 1 can be generalized[23,32] to a parameter, Λ, defined as:

$$\Lambda = \frac{\sum_{i,a} \kappa_{ia}^2 O_{ia}}{\sum_{i,a} \kappa_{ia}^2} \quad (2)$$

where, we have formed a sum of the overlaps of each occupied-virtual pair participating in a given transition, weighted by the percentage contribution from each orbital pair. Also, $\kappa_{ia} = (X_{ia} + Y_{ia})$, where X_{ia}'s and Y_{ia}'s correspond to excitations and de-excitations, respectively and are the eigen-vector elements of the TD-DFT equation.[44]

Table 3: Orbital overlap parameter,[23] Λ calculated using O_{ia} within the two approximations to *xc*-functional.

Dye	Λ_{B3LYP}	$\Lambda_{\mathrm{CAM-B3LYP}}$
TC1	0.57	0.54
L1	0.50	0.49
LJ1	0.52	0.51

The overlap parameter (Table 3) can be seen to follow the trend: $\Lambda^{TC1} > \Lambda^{LJ1} > \Lambda^{L1}$. One can see that the performance of B3LYP deteriorates as one goes from TC1 (excitation energy error=$\Delta E = -0.30\,\mathrm{eV}$[23]) to LJ1 ($\Delta E = -0.67\,\mathrm{eV}$[23]) to L1 ($\Delta E = -0.87\,\mathrm{eV}$[23]). The TD-DFT results within CAM-B3LYP are closer to the experimental values. Within CAM-B3LYP, the errors in the predicted excitation energies (relative to experimental value) are equal to $+0.18\,\mathrm{eV}$[23] for TC1, $-0.13\,\mathrm{eV}$[23] for L1 and $-0.03\,\mathrm{eV}$[23] for LJ1.

In the case of a dye meant to be adsorbed onto titania for DSSCs, it is important for the HOMO of the dye to lie within titania bandgap and the LUMO to lie within the conduction band. This is indeed the case for all three dyes as can be seen in Table 1, where we have also given the valence band maxima and conduction band minima of TiO_2 nanoparticle calculated within both B3LYP and CAM-B3LYP. It is clear from Table 1 that the orbital-energy bandgap of the nanoparticle is overestimated within B3LYP (E_g= 4.52 eV) and CAM-B3LYP (E_g= 7.57 eV) as compared to the experimental value[5] for the optical bandgap ($\sim$ 3.2 eV). In part, this broadening of the bandgap results from the quantum confinement effects that come into play in such a small nanoparticle. In fact, several experimental works[45–47] have reported this blue shift of the optical bandgap in TiO_2 nanoparticles that are a few nm in size. However, there is an additional source of bandgap broaden-

ing here. These highly exaggerated values can be attributed to the addition of HF-exchange, which is known to overestimate the band gaps. Upon inclusion of correlation effects (interaction between the excited electron and the hole) that is done within the framework of a TD-DFT calculation using hybrid functionals, the first transition energy decreases to a more reasonable value of $\sim$3.80 eV within B3LYP and to a still over-estimated value of $\sim$4.43 eV within CAM-B3LYP (also, see the discussion by Albert *et al.*[48]).

In spite of the overestimation of the titania bandgap within CAM-B3LYP, it is instructive to use both – B3LYP and CAM-B3LYP – functionals to study the dye-titania complexes. This choice of functionals can be justified as it is the dye that is the photoactive component within the complex and to describe the excitation properties of such molecules accurately one needs to correct the long-range behavior of the functionals by including a larger percentage of exact exchange (as is done in CAM-B3LYP). One consequence of this bandgap-opening is that there are fewer titania states in the conduction-band manifold below the LUMOs of the respective dyes. This, in turn, limits the number of states into which the photo-excited electron can be injected. In other words, there is a trade-off in using functionals such as CAM-B3LYP. They improve the description of excited state properties of one component of the complex, while doing just the opposite for the other half of the complex. This also limits the accuracy with which one can predict the nature of charge injection from the excited dye into titania. This injection of the photo-excited charge can take place through two mechanisms:

1. In direct CT mechanism, the photo-excited charge is injected from the dye to the conduction band of the semiconductor in one step. The empty states involved in this transition usually show a strong localization on the titania nanoparticle or a strong hybridization between the dye- and titania-states.

2. In case of indirect mechanism, the charge transfer is completed in two steps: (1) the charge is excited from the HOMO of the complex that is mostly localized on the dye to an empty state that is also localized mostly on the dye itself, and (2) then the charge tunnels into the conduction band manifold of the semiconductor.

In light of the above discussion, one may rightly deduce that the accuracy of level alignment will dictate the accuracy with which one may make predictions about the mechanism(s) involved in charge injection. The underestimation of HOMO-LUMO gap of the dye (as done by B3LYP) or the overestimation of the nanoparticle's bandgap (as done by CAM-B3LYP) may make such predictions less reliable. In the following section, we will discuss our results for the complex in greater details.

Titania-Dye Complexes

So far, we have described the electronic structures and the excited state properties of the isolated systems. The next step in this research was to look at the dye/titania complexes and study the excited state properties of the complexes. The functional choice is expected to affect both the ground and the excited state properties of the dye-titania complexes as well. This section is divided into two parts (not mutually exclusive) – in the first part, we briefly discuss the ground state properties, such as, dye-TiO_2 binding energies, ground state geometries and bond lengths within the two approximations. The second half of this section looks into the excited state properties of the dye adsorbed onto titania.

Ground State Properties: Effect of Functionals

The dye molecules are chemisorbed onto the nanoparticle through the acidic dissociation of the carboxylic acid anchor. In this process, hydrogen atom is removed from the carboxylic acid and bond formation takes place between carboxylate oxygen atoms and the five-fold coordinated titanium atoms on the surface of the metal oxide. To maintain the neutrality of the system, the hydrogen atom that was removed from the carboxylic acid, is transferred to one of the under-coordinated oxygen on titania surface. These structures were relaxed within B3LYP and CAM-B3LYP and were then used to study the effect of the two approximations to *xc*-functionals on the various ground state properties.

Table 4: Dye-titania binding energies (B.E) and O_{Dye} - $Ti_{Surface}$ bond lengths (B.L.) within different approximations.

Approx.	B.E. (eV)	B.L. (Å)
	TC1-TiO_2	
1) B3LYP	1.23	2.02, 2.12
2) CAM-B3LYP	1.36	2.04, 2.09
	L1-TiO_2	
1) B3LYP	1.27	2.02, 2.11
2) CAM-B3LYP	1.43	2.04, 2.10
	LJ1-TiO_2	
1) B3LYP	1.27	2.01, 2.11
2) CAM-B3LYP	1.41	2.04, 2.07

The strength of interaction between the organic dye and the metal-oxide nanoparticle can be characterized by their binding energies (B.E.). This can be calculated by subtracting the total energy of the complex ($E^{Complex}$) from the sum of energies of the isolated dye (E^{Dye}) and the isolated surface ($E^{Surface}$):

$$B.E. = [E^{Dye} + E^{Surface}] - E^{Complex} \tag{3}$$

Table 4 gives the binding energies of the two dyes with the titania surface as calculated within B3LYP and CAM-B3LYP. The binding energies show sensitivity to the choice of approximation to the *xc*-functional. As expected, the B.E. of the dye to the nanoparticle increases as one goes from B3LYP to CAM-B3LYP, owing to a larger amount of HF-exchange at long range in the latter.[48] Both functionals, however, show the same trend in the binding energies of the three dyes – the L1 and the LJ1-dyes show a slightly increased interaction with titania as compared to the TC1-dye.

In Table 4, we have also given the bond lengths between the dye's oxygen atoms (O_{Dye}) and the titanium atoms ($Ti_{Surface}$) on the surface to which the dyes bind upon chemisorption. Although, the starting geometries for all structures had very similar bond lengths (~ 2.02) between these atoms, the relaxed geometries are different. In case of B3LYP, the lengths of the two bonds are more dissimilar than in the case of CAM-B3LYP.

Excited-State Properties: Effect of Functionals

After the structural optimization, TD-DFT calculations were carried out for the different structures. Figure 4 shows the UV/Vis spectra for the two complexes as calculated within B3LYP and CAM-B3LYP. Table 5 gives details of the important transitions (corresponding to $\lambda_{max}^{Th.}$) and the states involved in the transition. Unlike, the isolated dye, the most prominent transitions do not necessarily involve the HOMO-LUMO pair, but may involve higher states.

Table 5: Details of transitions corresponding to $\lambda_{max}^{Th.}$ and a few of the comparable peaks for the dye-titania complexes.

Dyes Approx.	T. E. (eV) (O.S.)	Involved Orbitals (Coeff.)
TC1-TiO_2		
1) B3LYP	2.45 (0.11)	H→L+3 (0.10), H→L+4 (0.24), H→L+5 (0.54), H→L+6 (0.16), H→L+7 (0.22), H→L+8 (0.19)
	2.47 (0.13)	H→L+3 (0.17), H→L+5 (0.25), H→L+6 (0.16) H→L+7 (0.60)
	2.59 (0.16)	H→L+8 (0.15), **H→L+10 (0.52)**, H→L+11 (0.19) H→L+12 (0.33), H→L+13 (0.17)
	2.67 (0.11)	H→L+14 (0.35), H→L+15 (0.54), H→L+16 (0.26)
	2.70 (0.13)	H→L+14 (0.31), H→L+16 (0.57), H→L+17 (0.19)
2) CAM-B3LYP	**3.17 (1.43)**	H→L+2 (0.17), H→L+3 (0.34), H→L+4 (0.18) **H→L+5 (0.48)**
L1-TiO_2		
1) B3LYP	**2.08 (0.88)**	H→L+1 (0.15), H→L+2 (0.21), **H→L+3 (0.52)** H→L+4 (0.39), H→L+5 (0.10)
2) CAM-B3LYP	**2.87 (1.51)**	H-1→L (0.27), **H→L (0.61)**
LJ1-TiO_2		
1) B3LYP	**2.05 (0.48)**	H→L+2 (0.16), H→L+3 (0.39), **H→L+4 (0.48)** H→L+5 (0.26)
	2.09 (0.32)	H→L+4 (0.16), H→L+5 (0.54), H→L+6 (0.40)
2) CAM-B3LYP	**2.79 (1.55)**	H-1→L (0.24), H-1→L+1(0.12), **H→L (0.55)** H→L+1 (0.28)

TC1-TiO_2 Complex

The experimental UV/Vis absorption spectrum shows a maximum absorbance at energy of ~ 2.94 eV for TC1-surface complexes.[33] Theoretically calculated spectra for this dye-titania complex show

absorption maxima at ~ 2.59 eV within B3LYP and at ~ 3.17 eV within CAM-B3LYP (see, Table 5 and Figure 5). CAM-B3LYP improves the description of the excited state properties, yielding an error of $\Delta E^{\mathrm{CAM-B3LYP}} = 0.23$ eV in the excitation energy as compared to the B3LYP result ($\Delta E^{\mathrm{B3LYP}} = -0.35$ eV).

The absorption spectrum calculated using B3LYP, not only shows an underestimation of the excitation energy, but also shows an overcrowding of the spectrum with many prominent transitions (Figure 4), although all with small oscillator strengths (see, Table 5). The unoccupied molecular orbitals (MOs) that participate in these major transitions range from LUMO+3 to LUMO+17. Figure 6 shows the major occupied-empty orbitals involved in the transition with the largest oscillator strength. The HOMO of the complex is mostly derived from the HOMO of the dye. On the other hand, LUMO+10 shows very small contribution from the dye. For the sake of brevity, other orbitals involved in the major transitions are not shown here. However, we have plotted the planar-averages of the charge densities (absolute values) of the main MOs involved in major transitions. These plots contain similar information to the three-dimensional rendition of MOs, but in a rather succinct way. The planar averages of the charge densities can be defined as:

$$\bar{n}(z) = \frac{1}{\Sigma_{xy}} \int |n((r))|\, dx\, dy \tag{4}$$

Here, $\bar{n}(z)$ is the planar-averaged charge density along the z-direction as shown in Figure 6, Σ_{xy} is the area of the xy-plane and $|n((r))|$ is the absolute value of the charge density. Figure 7(a) shows planar averages of the charge densities for a few of the MOs of the complex involved in photo-excitations. There is no unique way to choose the boundary between the two sub-systems. Here, the hydrogen atom on the surface of titania is chosen to be the zero of the axis. Most of the unoccupied states involved in the major transitions can be seen to a have only a small contribution from the dye and are mostly localized on the TiO_2 nanoparticle.

In contrast to the B3LYP results, CAM-B3LYP spectrum for the TC1-TiO_2 complex shows only one prominent peak at an energy of 3.17 eV. Figure 6 shows the isosurface plots of the major MOs involved in the transition. The promotion from the HOMO to the LUMO+5 orbital has the

largest percentage contribution in the transition. The hybridization of the states derived from *3d*-states of titanium and the LUMO of the isolated dye gives rise to the unoccupied state, LUMO+5. There are several other states that also participate in the photo-excitation [Figure 7(b)] and they also show strong hybridization between the LUMO of the isolated dye and the *3d*-derived states of titania.

Although, the details are different, both B3LYP and CAM-B3LYP predict direct charge transfer as the major mechanism for charge injection from the excited dye into titania.

L1-TiO_2 Complex

The experimental UV/Vis absorption spectrum shows a maximum absorbance at energy of ~ 3.07 eV for L1-surface complexes.[30,34] As, it was seen in an earlier section on the isolated dyes, B3LYP's performance deteriorates as one goes from a dye with a larger orbital overlap (TC1) to the L1-dye that shows a much smaller overlap between the frontier orbitals. As it is the dye that is the photoactive component of the complex, it is expected that this trend is seen in their complexed form also. We find that this is indeed the case. The TD-DFT calculation within B3LYP underestimates the absorption maximum to be at ~ 2.08 eV, giving a very large error of -0.99 eV. The range-separated functional, CAM-B3LYP, improves upon these results [$\lambda_{max}^{\mathrm{CAM-B3LYP}} = 2.87$ eV], giving an error of -0.20 eV (see, Table 5 and Figure 8). This shows the importance of determining the right functional for the photoactive component before using a particular functional for studying a more complex structure such as dyes adsorbed onto semiconductor nanoparticle/films or dyes within supramolecules.

The absorption spectrum calculated using B3LYP shows one prominent transition (Figure 4) with large oscillator strength (see, Table 5). All promotions take place from the HOMO of the complex to several of the empty states that range from LUMO+1 to LUMO+5. The largest percentage contribution in this excitation comes from LUMO+3. Figure 9 shows the HOMO and LUMO+3 of L1-TiO_2 complex. The HOMO of the complex is mostly derived from the HOMO of the dye. On the other hand, LUMO+3 shows hybridization of the LUMO of the isolated L1-dye and the titania

states derived from *3d*-states of titanium. We have also plotted the planar averages of the charge densities (absolute values) of the main MOs involved in this transition. Figure 10(a) shows planar averages of the (absolute) charge densities for a few of the major MOs that are involved in photo-excitation. From the plot one can see that the HOMO of the complex is mostly located on the dye. Out of the empty states, LUMO+2 and LUMO+1 (not shown in the diagram to avoid crowding of the plot) are mostly localized on titania, while the others have considerable contribution from both the dye and the nanoparticle. B3LYP predicts a direct charge transfer as the dominant mechanism at play in the L1-TiO_2 complex.

The results from the TD-DFT calculation within CAM-B3LYP are very different from their B3LYP counterparts. The most prominent excitation (see, Table 5) shows two promotions: HOMO-1→LUMO, and HOMO →LUMO. The two occupied orbitals of the complex – HOMO-1 (not shown here) and HOMO (Figure 9) – are both localized on the dye. The empty state of the complex involved in the transition is derived mostly from the dye's LUMO and has some contribution from the surface states of titania. Such a result for any other complex might mean that the two mechanisms – direct and indirect CT – may co-exist and contribute to charge injection. However, the latter mechanism is not possible for the particular case of L1-complex as the empty state involved in the excitation is also the LUMO of the complex; the excited charge cannot tunnel into other empty states. This is due to the overestimation of titania's bandgap within CAM-B3LYP, showing the limits of applying such an approximation to these structures. This overestimation, in turn, results in inaccurate alignment of states and the LUMO of L1 is almost at the edge of titania's conduction band. This overestimation of titania's bandgap within CAM-B3LYP was not a very critical problem for the case of TC1-TiO_2 complex. The difference between the TC1-dye and the L1-dye is that in the former case, the HOMO-LUMO gap of the isolated dye has a much larger value of 5.42 eV (see, Figure 6), resulting in at least a few more empty states below the unoccupied states that are involved in the excitation within TC1-TiO_2 complex. On the other hand, the HOMO-LUMO gap for L1 is only 4.77 eV, putting the dye's LUMO at titania's conduction band edge (see, Table 1). Thus, the CT mechanism cannot be accurately predicted in the case

the L1-TiO_2 complex. In other words, the use of CAM-B3LYP improves the excitation energies predicted for the isolated L1-dye and the L1-TiO_2 complex at the cost of our ability to predict the CT mechanism accurately. The B3LYP approximation also does not perform too well for L1-TiO_2 complex (excitation-energy error, $\Delta E^{\mathrm{B3LYP}} = -0.99\,\mathrm{eV}$). and the results within B3LYP cannot be used reliably. Thus, the robustness of the TD-DFT results depends critically on the choice of functionals and one can not use just one approximation, such as, B3LYP or even, CAM-B3LYP for all systems. In the case of dyes such as L1, it becomes important to explore other range-separated functionals that may perform better for titania, while at least performing as well for the dye as the CAM-B3LYP approximation.

LJ1-TiO_2 Complex

The experimental UV/Vis absorption spectrum shows a maximum absorbance at energy of $\sim 2.76\,\mathrm{eV}$ for LJ1-surface complexes.[34] The TD-DFT calculation within B3LYP underestimates the absorption maximum to be at $\sim 2.05\,\mathrm{eV}$, giving a very large error of -0.71 eV. On the other hand, CAM-B3LYP functional gives a very accurate value of 2.79 eV for the CT excitation energy, giving an error of -0.03 eV (see, Table 5 and Figure 11).

The absorption spectrum calculated using B3LYP shows a couple of prominent transitions (Figure 4) with large oscillator strengths (see, Table 5). All promotions take place from the HOMO of the complex to several of the empty states that range from LUMO+2 to LUMO+6. The largest percentage contribution in the main excitation (corresponding to λ_{max}^{B3LYP}) comes from LUMO+4. Figure 12 shows the HOMO and LUMO+4 of LJ1-TiO_2 complex. The HOMO of the complex is mostly derived from the HOMO of the dye. LUMO+4 shows contributions from both sub-systems of the complex. It is derived from the LUMO of the LJ1-dye and the titania states derived from *3d*-states of titanium. Figure 13(a) shows planar averages of the (absolute) charge densities for a few of the major MOs that are involved in photo-excitation. From the plot one can see that the HOMO of the complex is mostly located on the dye. Out of the empty states, LUMO+2 and LUMO+3 are mostly localized on titania, while the others have considerable contribution from both the dye and

the nanoparticle. B3LYP once again predicts the direct charge transfer as the dominant mechanism for the charge injection from the dye into the nanoparticle.

The TD-DFT calculation within CAM-B3LYP shows only one main peak. This excitation (see, Table 5) shows contributions from several promotions within filled states (HOMO-1 and HOMO) and the empty states (LUMO and LUMO+1). The two occupied orbitals of the complex – HOMO-1 (not shown here) and HOMO (Figure 12) are mostly derived from the HOMO-1 and HOMO of the dye, respectively. The empty states of the complex involved in the transition are formed from the hybridization of dye's LUMO and the *3d*-states of titanium. This can also be seen from Figure 13(b) that shows planar averages of the (absolute) charge densities for the MOs that are involved in photo-excitation. These results show that the direct charge transfer is the dominant mechanism for the charge-injection process within the complex.

It is interesting to note that the CAM-B3LYP results are more reliable for the complex of LJ1 than for the complex of L1. In part this is a result of slightly better alignment of dye's LUMO within titania's conduction band (see, Table 1 for positions of LUMOs). In addition, the performance of a given approximation for the isolated dyes is indicative of how well it will predict the values of excitation energies for the complexes. This can be seen in the cases of all three dyes and their complexes considered here (see, Table 6). In the dye-titania complex, it is the dye is that absorbs in the visible range. It is, therefore, important to first determine the most appropriate functional for the given dye before proceeding to study it in larger, more complex structures.

Discussion

In this work, we have explored the functional performance in predicting the charge-transfer excitation energies in triphenylamine-donor dyes in isolation and in a complex with the anatase titania nanoparticle. These dyes and their derivatives are of interest for dye-sensitized solar cells. As such, it is imperative to simulate the structural and electronic properties of these systems accurately. The TPA-dyes were also chosen as it is hard to capture the right photo-physics of these dyes using

Table 6: Excitation Energy Errors [$\Delta E^{\text{Approx.}} = E^{\text{Th.}} - E^{\text{Expt.}}$] in eV. The accuracy of the results for isolated dyes is indicative of the functional performance for dye-titania complexes.

Dye/ Approx.	Isolated Dye	Complex
TC1		
ΔE^{B3LYP}	-0.30	-0.35
$\Delta E^{\text{CAM-B3LYP}}$	0.18	0.23
L1		
ΔE^{B3LYP}	-0.87	-0.99
$\Delta E^{\text{CAM-B3LYP}}$	-0.13	-0.20
LJ1		
ΔE^{B3LYP}	-0.67	-0.71
$\Delta E^{\text{CAM-B3LYP}}$	-0.03	-0.03

local, semi-local or conventional hybrid functionals. The B3LYP approximation to the exchange correlation functional fails to a varying degree in its description of charge transfer excitation in the isolated dyes. As it is the dye that absorbs in the visible range (spectral range of interest in solar cells) when complexed with titania, this failure of B3LYP is propagated in its predicted values of the charge transfer excitation energies of the complexes. One needs to use CAM-B3LYP to capture the correct photophysics of the dyes and to get accurate charge-transfer excitation energies of their complexes with titania. This work shows the importance of carefully choosing the most appropriate functional to study a given system. As the dye-titania complexes or supramolecules containing such dyes are very large systems, it is computationally expensive to carry out such functional assessments in these structures. However, one may proceed by determining the most appropriate functional for the isolated dye and then study it in complexed-form, using results for the former as a guideline. Hence, this research provides a simple course of action for exploring charge-transfer excitation of very complicated structures where only one component is photoactive in the desired spectral range.

Although, we have explored only two of the many approximations to the *xc*-functional, this work also highlights several issues with this field of research:

1. TD-DFT can yield reasonably accurate results (with errors as small as a few tenths of an

eV) if one chooses a functional that is most appropriate for the problem. In other words, using only functionals such as B3LYP, which is a common practice in the field, may lead to erroneous results. One may use the overlap parameter as defined in the work by Peach *et al.*[32] to obtain the important information about the "degree" of CT involved in a transition. This, in turn, can help to determine the suitability of a functional for the dye of interest.

2. In particular, it is not possible to simultaneously obtain both accurate CT excitation energies of the dye-titania complexes and reasonable level alignment within the two approximations explored here. Although, B3LYP underestimates the CT excitations of the isolated dyes and their complexes, it gives better description of the bandstructure of titania nanoparticle. CAM-B3LYP achieves just the opposite. Overall, CAM-B3LYP is still a better choice for predicting CT excitation energies. However, this may come at the cost of accuracy with which one can predict the nature of charge transfer mechanism itself. For instance, in case of the CAM-B3LYP calculation for L1-TiO_2 complex, the LUMO of the complex is derived mostly from the dye's LUMO, with only a very small contribution from the *3d*-states of the surface titanium atoms. In all appearances, this would indicate indirect CT as the prominent injection mechanism. However, it is not a possibility for this system as there are no lower empty states into which the photo-excited electron can be injected through tunneling. The absence of a *3d*-state derived conduction-band manifold below this level is just an artifact of our use of CAM-B3LYP approximation – CAM-B3LYP overestimates titania's bandgap to a very large extent. This makes it difficult to conclusively predict the CT mechanism for L1-TiO_2 complex.

In order to overcome the aforementioned shortcomings, it will be instructive if the performance of other long-range corrected functionals is explored as well. A careful choice of functional, in turn, will help to calculate various system properties accurately. Finally, it is also worth mentioning that although computationally cheaper, TD-DFT is not the only method to calculate the absorption spectra. It will be interesting to compare the TD-DFT results with those obtained within GW-Bethe-Salpeter (GW-BSE) method. The latter is a much more expensive calculation that can

provide a more accurate description of the excited state properties.

Acknowledgement

We acknowledge the computational support provided by the Irish Centre for High-End Computing (ICHEC). PD acknowledges financial support for this work through EMPOWER fellowship granted by Irish Research Council for Science and Engineering (IRCSET). SA is supported by the Science Foundation Ireland under Grant No. [07/SRC/B1160].

References

(1) O'Regan, B.; Grätzel, M. *Nature* **1991**, *353*, 737–740.

(2) Grätzel, M. *J. Photochem. Photobio. C: Photochem. Reviews* **2003**, *4*, 145–153.

(3) Listorti, A.; O'Regan, B.; Durrant, J. R. *Chem. Mat.* **2011**, *23*, 3381–3399.

(4) Hagfeldt, A.; Boschloo, G.; Sun, L.; Kloo, L.; Pettersson, H. *Chem. Rev.* **2010**, *110*, 6595–6663.

(5) Kavan, L.; Grätzel, M.; Gilbert, S. E.; Klemenz, C.; Scheel, H. J. *J. Am. Chem. Soc.* **1996**, *118*, 6716–6723.

(6) Grätzel, M. *J. Photochem. Photobiol. A: Chem.* **2004**, *164*, 3–14.

(7) Nazeeruddin, M. K.; De Angelis, F.; Fantacci, S.; Selloni, A.; Viscardi, G.; Liska, P.; Ito, S.; Takeru, B.; Grätzel, M. *J. Am. Chem. Soc.* **2005**, *127*, 16835–16847.

(8) Nazeeruddin, M. K.; Kay, A.; Rodicio, I.; Humphrybaker, R.; Muller, E.; Liska, P.; Vlachopoulos, N.; Grätzel, M. *J. Am. Chem. Soc.* **1993**, *115*, 6382–6390.

(9) Mishra, A.; Fischer, M. K.; Bauerle, P. *Angew. Chem. Int. Ed. Engl.* **2009**, *48*, 2474–2499.

(10) Tian, H.; Meng, F. *Organic Photovoltaics: Mechanisms, Materials, and Devices*; Eds.: S. S. Sun, N. S. Sariciftci, CRC, London, 2005; pp 313–330.

(11) Persson, P.; Bergstrom, R.; Lunell, S. *J. Phys. Chem. B* **2000**, *104*, 10348–10351.

(12) De Angelis, F.; Tilocca, A.; Selloni, A. *J. Am. Chem. Soc.* **2004**, *126*, 15024–15025.

(13) Duncan, W. R.; Prezhdo, O. V. *J. Phys. Chem. B* **2005**, *109*, 365–373.

(14) Duncan, W. R.; Stier, W. M.; Prezhdo, O. V. *J. Am. Chem. Soc.* **2005**, *127*, 7941–7951.

(15) Duncan, W. R.; Prezhdo, O. V. *Annu. Rev. Phys. Chem.* **2007**, *58*, 143–184.

(16) De Angelis, F.; Fantacci, S.; Selloni, A.; Grätzel, M.; Nazeeruddin, M. K. *Nano Lett.* **2007**, *7*, 3189–3195.

(17) Pastore, M.; Angelis, F. D. *ACS Nano* **2010**, *4*, 556–562.

(18) Rocca, D.; Gebauer, R.; Angelis, F. D.; Nazeeruddin, M. K.; Baroni, S. *Chem. Phys. Lett.* **2009**, *475*, 49 – 53.

(19) De Angelis, F. *Chem. Phys. Lett.* **2010**, *493*, 323–327.

(20) De Angelis, F.; Fantacci, S.; Mosconi, E.; Nazeeruddin, M. K.; Grätzel, M. *J. Phys. Chem. C* **2011**, *115*, 8825–8831.

(21) Agrawal, S.; Dev, P.; English, N. J.; Thampi, K. R.; MacElroy, J. M. D. *J. Mater. Chem.* **2011**, *21*, 11101–11108.

(22) Agrawal, S.; Dev, P.; English, N. J.; Thampi, K. R.; MacElroy, J. M. D. *Chem. Sci.* **2012**, *3*, 416–424.

(23) Dev, P.; Agrawal, S.; English, N. J. *J. Chem. Phys* **2012**, *136*, 224301–1–224301–11.

(24) Perdew, J. P.; Burke, K.; Ernzerhof, M. *Phys. Rev. Lett.* **1996**, *77*, 3865–3868.

(25) Becke, A. D. *J. Chem. Phys.* **1993**, *98*, 5648–5652.

(26) Lee, C.; Yang, W.; Parr, R. G. *Phys. Rev. B* **1988**, *37*, 785–789.

(27) Stephens, P. J.; Devlin, F. J.; Ashvar, C. S.; Chabalowski, C. F.; Frisch, M. J. *Faraday Discuss.* **1994**, *99*, 103–119.

(28) Dreuw, A.; Head-Gordon, M. *J. Am. Chem. Soc.* **2004**, *126*, 4007–4016.

(29) Dreuw, A.; Head-Gordon, M. *Chem. Rev.* **2005**, *105*, 4009–4037.

(30) Hagberg, D. P.; Marinado, T.; Karlsson, K. M.; Nonomura, K.; Qin, P.; Boschloo, G.; Brinck, T.; Hagfeldt, A.; Sun, L. *J. Org. Chem.* **2007**, *72*, 9550–9556.

(31) Yanai, T.; Tew, D. P.; Handy, N. C. *Chem. Phys. Lett.* **2004**, *393*, 51 – 57.

(32) Peach, M. J. G.; Benfield, P.; Helgaker, T.; Tozer, D. J. *J. Chem. Phys* **2008**, *128*, 044118–1–044118–8.

(33) Xu, W.; Peng, B.; Chen, J.; Liang, M.; Cai, F. *J. Phys. Chem. C* **2008**, *112*, 874–880.

(34) Liu, W.-H.; Wu, I.-C.; Lai, C.-H.; Lai, C.-H.; Chou, P.-T.; Li, Y.-T.; Chen, C.-L.; Hsu, Y.-Y.; Chi, Y. *Chem. Commun.* **2008**, 5152–5154.

(35) Chen, B.-S.; Chen, D.-Y.; Chen, C.-L.; Hsu, C.-W.; Hsu, H.-C.; Wu, K.-L.; Liu, S.-H.; Chou, P.-T.; Chi, Y. *J. Mater. Chem.* **2011**, *21*, 1937–1945.

(36) Hwang, S.; Lee, J. H.; Park, C.; Lee, H.; Kim, C.; Park, C.; Lee, M.-H.; Lee, W.; Park, J.; Kim, K.; Park, N.-G.; Kim, C. *Chem. Commun.* **2007**, 4887–4889.

(37) Dreuw, A.; Weisman, J. L.; Head-Gordon, M. *J. Chem. Phys* **2003**, *119*, 2943–2946.

(38) Tozer, D. J. *J. Chem. Phys* **2003**, *119*, 12697–12699.

(39) Gritsenko, O.; Baerends, E. J. *J. Chem. Phys* **2004**, *121*, 655–660.

(40) Neugebauer, J.; Gritsenko, O.; Baerends, E. J. *J. Chem. Phys* **2006**, *124*, 214102–1–214102–11.

(41) Frisch, M. J. et al. Gaussian 09 Revision A.1. Gaussian Inc. Wallingford CT 2009.

(42) Cossi, M.; Rega, N.; Scalmani, G.; Barone, V. *J. Comp. Chem.* **2003**, *24*, 669–681.

(43) Izmaylov, A. F.; Scuseria, G. E. *J. Chem. Phys* **2008**, *129*, 034101.

(44) Casida, M. E. *RECENT ADVANCES IN DENSITY FUNCTIONAL METHODS (Part I), edited by Delano P. Chong*; Singapore, World Scientific, 1995; pp 155–192.

(45) Kormann, C.; Bahnemann, D. W.; Hoffmann, M. R. *J. Phys. Chem.* **1988**, *92*, 5196–5201.

(46) Weng, Y.-X.; Wang, Y.-Q.; Asbury, J. B.; Ghosh, H. N.; Lian, T. *J. Phys. Chem. B* **1999**, *104*, 93–104.

(47) Khoudiakov, M.; Parise, A. R.; Brunschwig, B. S. *J. Am. Chem. Soc.* **2003**, *125*, 4637–4642.

(48) Albert, V. V.; Ivanov, S. A.; Tretiak, S.; Kilina, S. V. *J. Phys. Chem. C* **2011**, *115*, 15793–15800.

Graphical TOC Entry

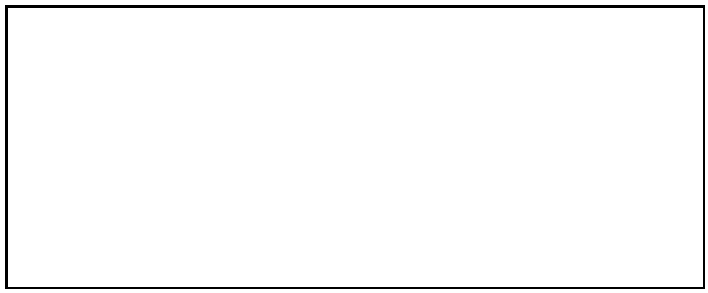

Figure 1: TPA-donor dyes: (a) TC1 (b) L1, and (c) LJ1

Figure 2: UV/Vis Spectra of TC1, L1, and LJ1 calculated within the B3LYP and CAM-B3LYP approximations to *xc*-functional.

Figure 3: Frontier Molecular Orbitals involved in photo-excitation: (a) HOMO of TC1, and (b) LUMO of TC1; (c) HOMO of L1, and (d) LUMO of L1; (e) HOMO of LJ1, and (f) LUMO of LJ1. The orbitals shown were calculated within CAM-B3LYP

Figure 4: UV/Vis Spectra of TC1-TiO_2, L1-TiO_2 and LJ1-TiO_2 complexes calculated within the B3LYP and CAM-B3LYP approximations, showing individual transitions as impulses.

Figure 5: Energy level diagram showing alignment of levels corresponding to the molecular orbitals of the TC1-dye (in blue), TiO_2 (in red) and TC1-TiO_2 complex (in grey) within (a) B3LYP and (b) CAM-B3LYP. Values given in parenthesis refer to the TD-DFT excitation energies. The states involved in the transition within the complex are shown with slightly longer lines.

Figure 6: Molecular orbitals of TC1-TiO_2 complex involved in transition corresponding to corresponding to $\lambda_{max}^{Th.}$ within B3LYP: (a) HOMO and (b) LUMO+10; and within CAM-B3LYP: (c) HOMO and (d) LUMO+5

Figure 7: Planar average charge densities corresponding to the TC1-TiO_2 orbitals involved in some important transitions within (a) B3LYP and (b) CAM-B3LYP approximations.

Figure 8: Energy level diagram showing alignment of levels corresponding to the molecular orbitals of the L1-dye (in blue) , TiO_2 (in red) and L1-TiO_2 complex (in grey) within (a) B3LYP and (b) CAM-B3LYP.

Figure 9: Molecular orbitals of L1-TiO_2 complex involved in transition corresponding to corresponding to $\lambda_{max}^{Th.}$ within B3LYP: (a) HOMO and (b) LUMO+3; and within CAM-B3LYP: (c) HOMO and (d) LUMO

Figure 10: Planar average charge densities corresponding to the L1-dye orbitals involved in some important transitions within (a) B3LYP and (b) CAM-B3LYP approximations.

Figure 11: Energy level diagram showing alignment of levels corresponding to the molecular orbitals of the LJ1-dye (in blue), TiO_2 (in red) and LJ1-TiO_2 complex (in grey) within (a) B3LYP and (b) CAM-B3LYP.

Figure 12: Molecular orbitals of LJ1-TiO_2 complex involved in transition corresponding to corresponding to $\lambda_{max}^{Th.}$ within B3LYP: (a) HOMO and (b) LUMO+4; and within CAM-B3LYP: (c) HOMO and (d) LUMO

Figure 13: Planar average charge densities corresponding to the LJ1-dye orbitals involved in some important transitions within (a) B3LYP and (b) CAM-B3LYP approximations.

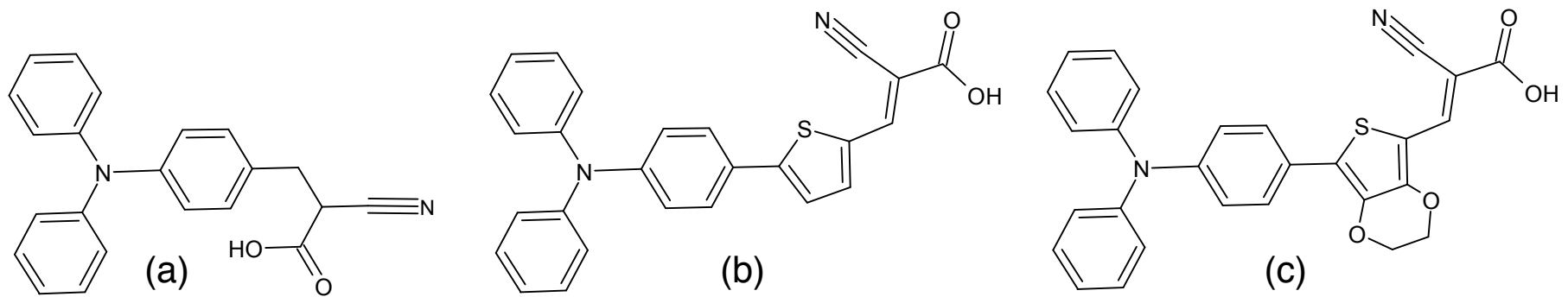
N
HO
O
N
(a)
N
S
O
OH
N
(b)
N
S
O
O
O
N
OH
N
(c)

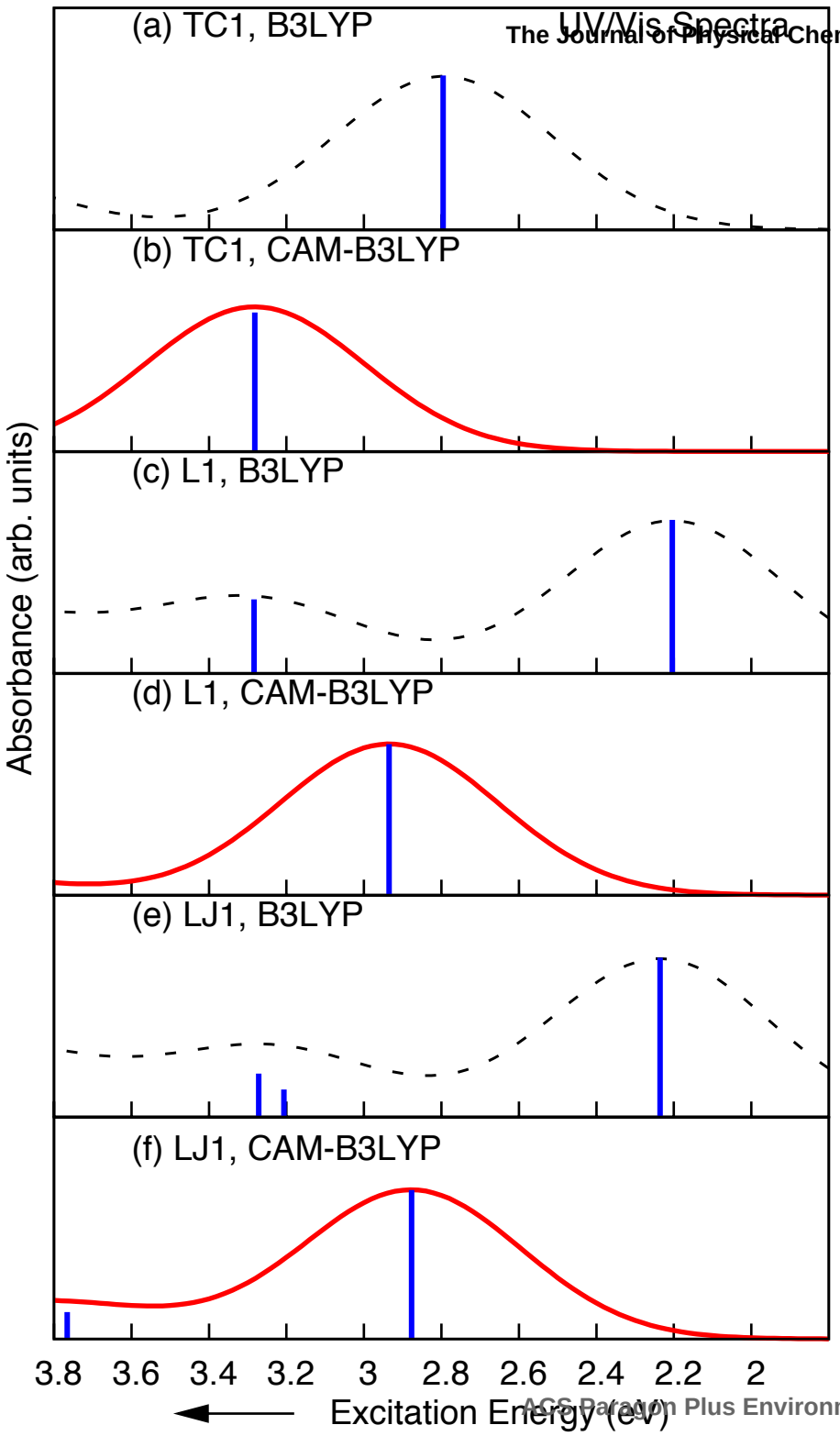

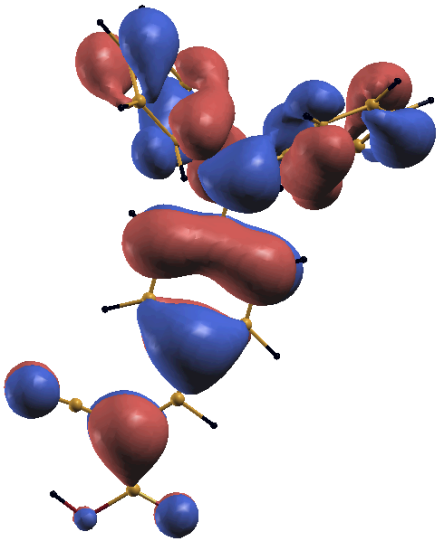

(a) TC1 HOMO

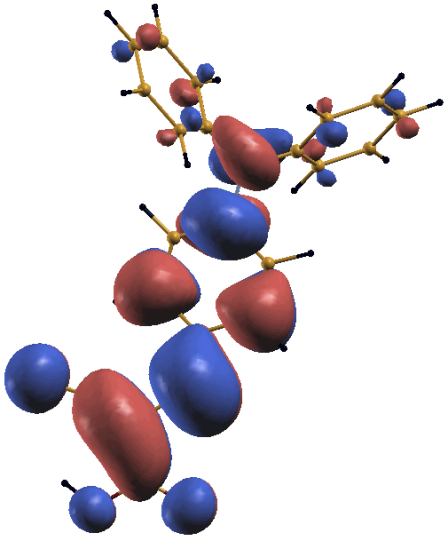

(b) TC1 LUMO

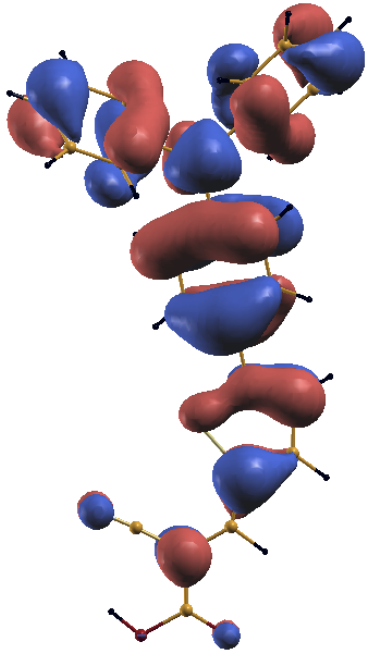

(c) L1 HOMO

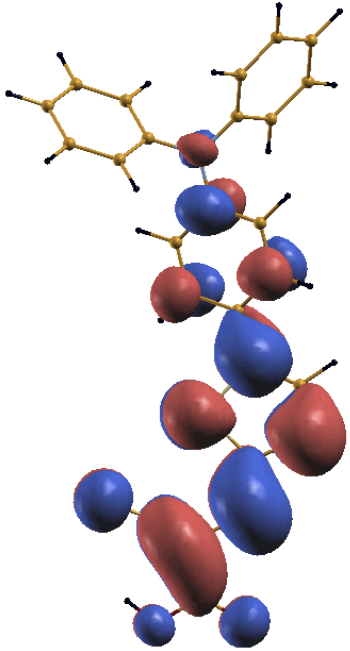

(d) L1 LUMO

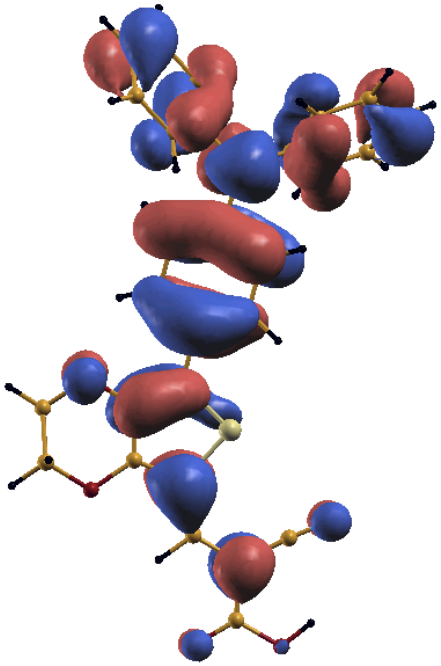

(e) LJ1 HOMO

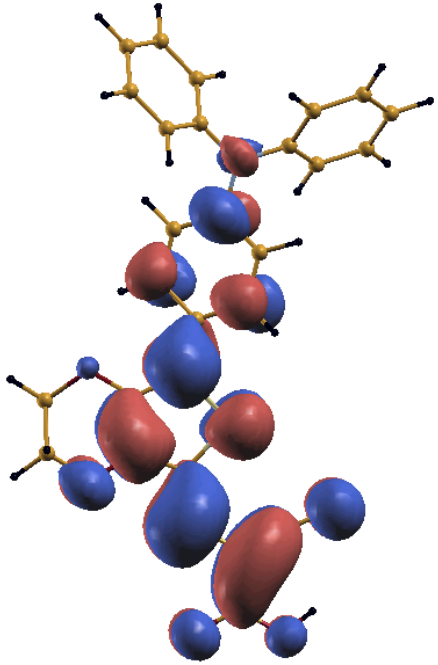

(f) LJ1 LUMO

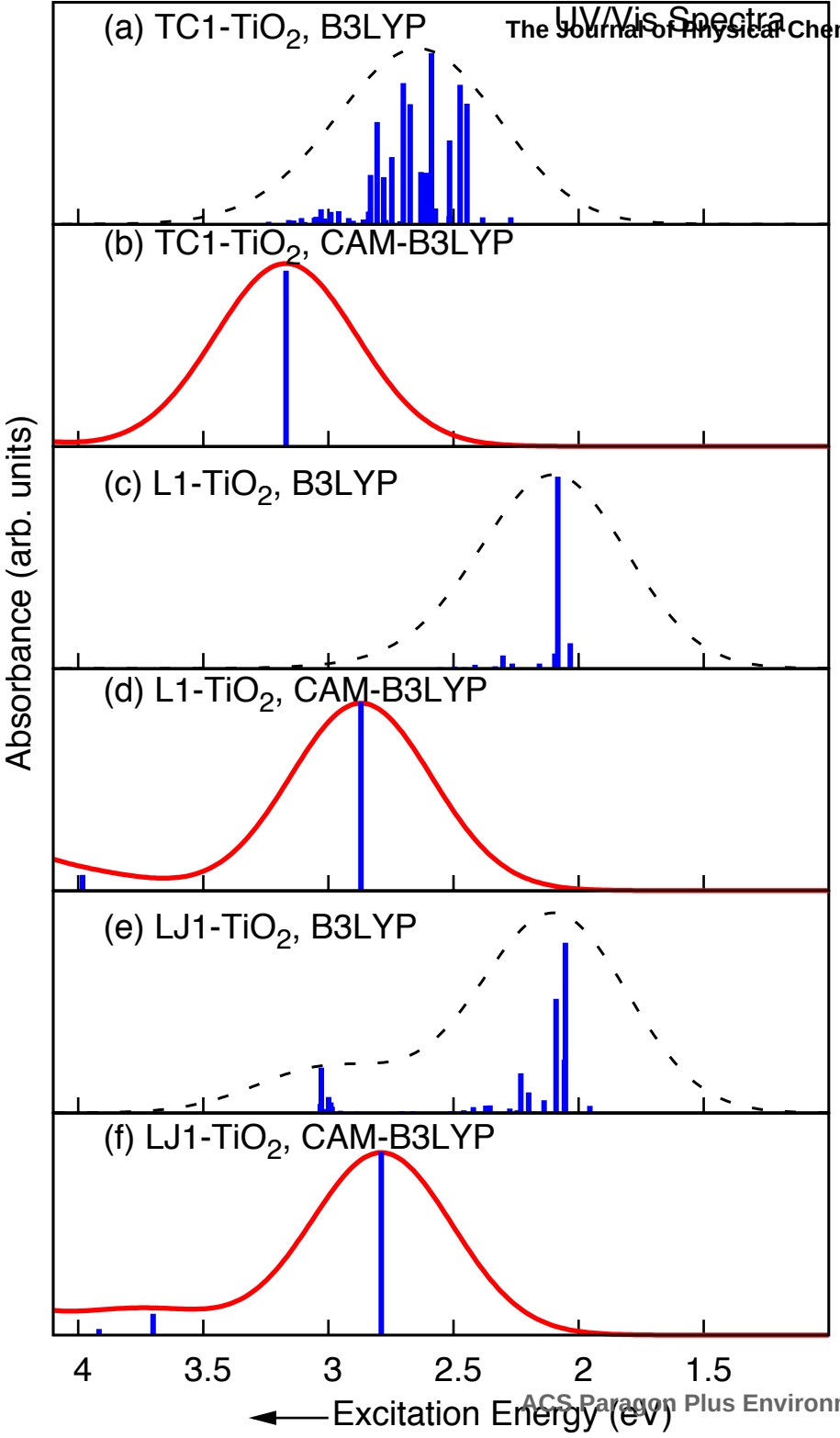

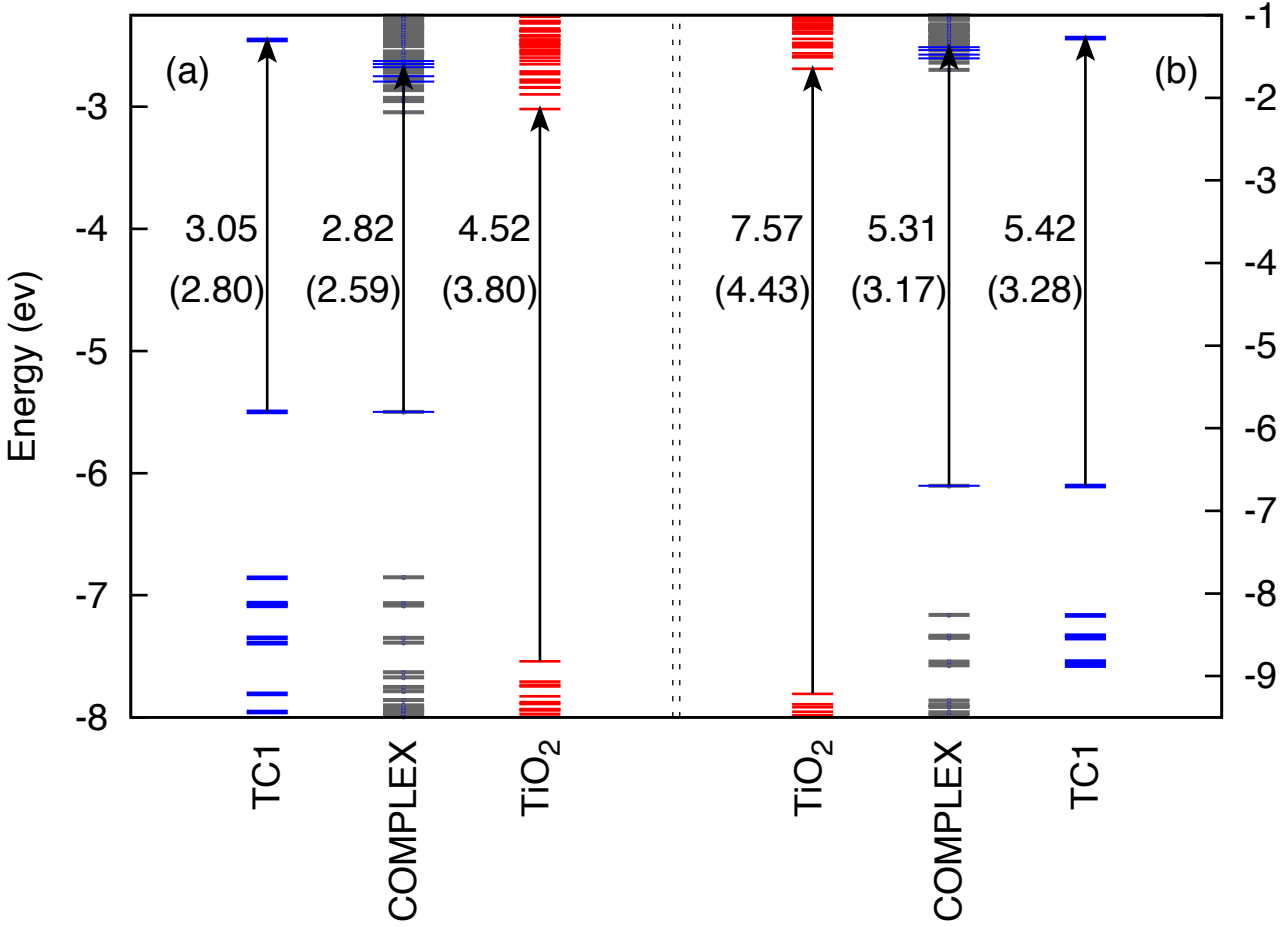
(a)
(b)
Energy (ev)
-1
-2
-3
-4
-5
-6
-7
-8
-9
3.05
(2.80)
2.82
(2.59)
4.52
(3.80)
7.57
(4.43)
5.31
(3.17)
5.42
(3.28)
TC1
COMPLEX
TiO2
TiO2
COMPLEX
TC1

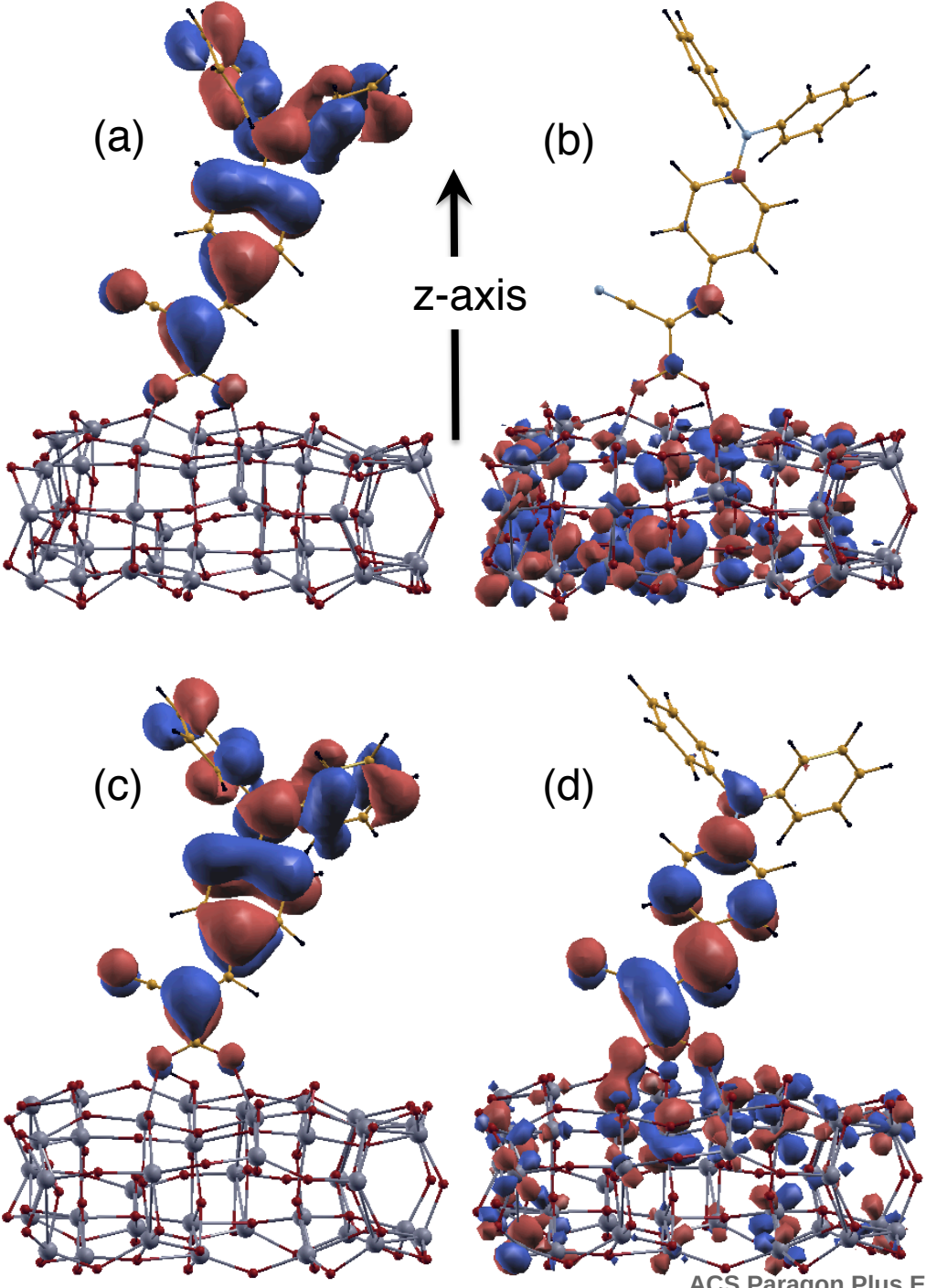

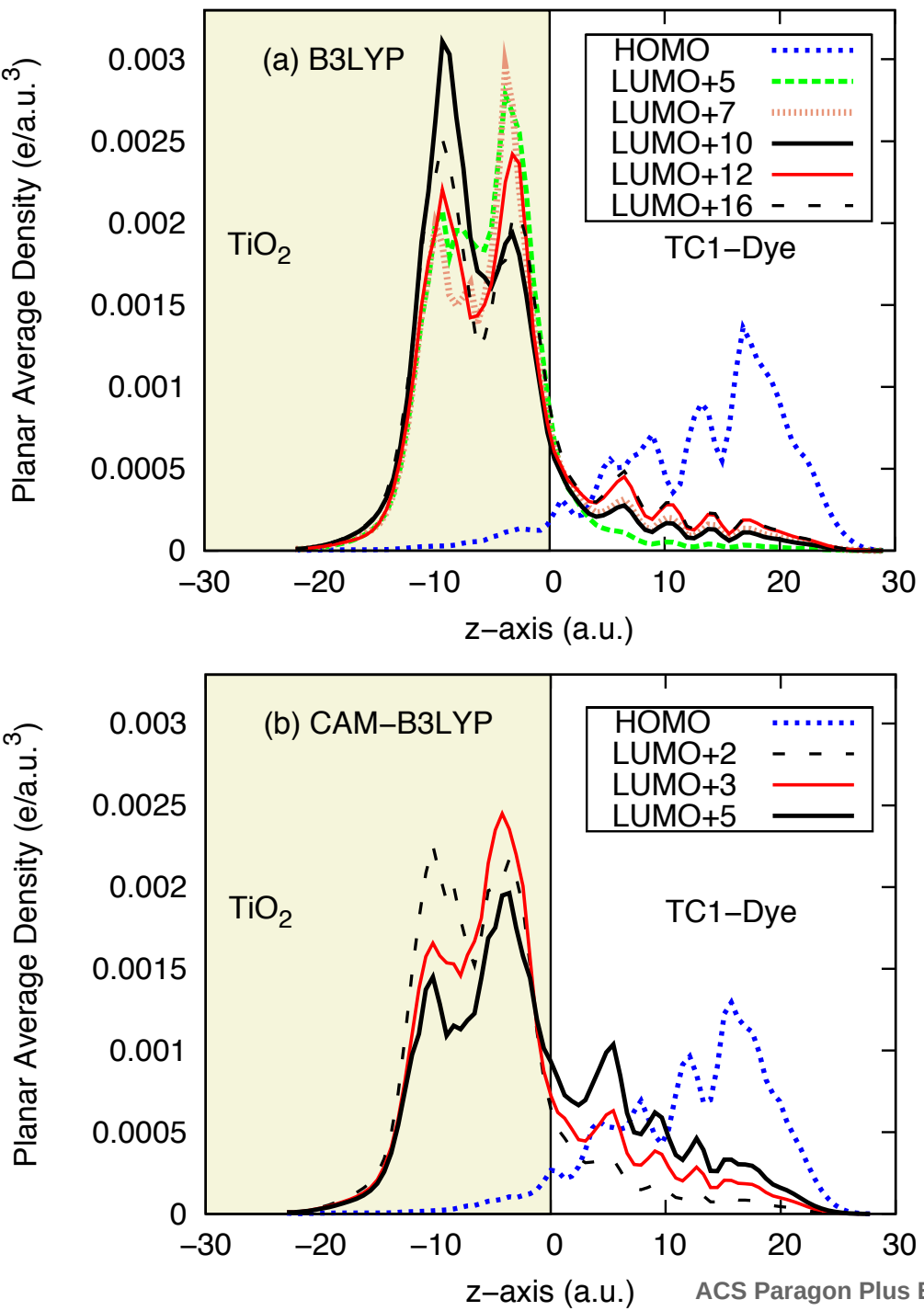

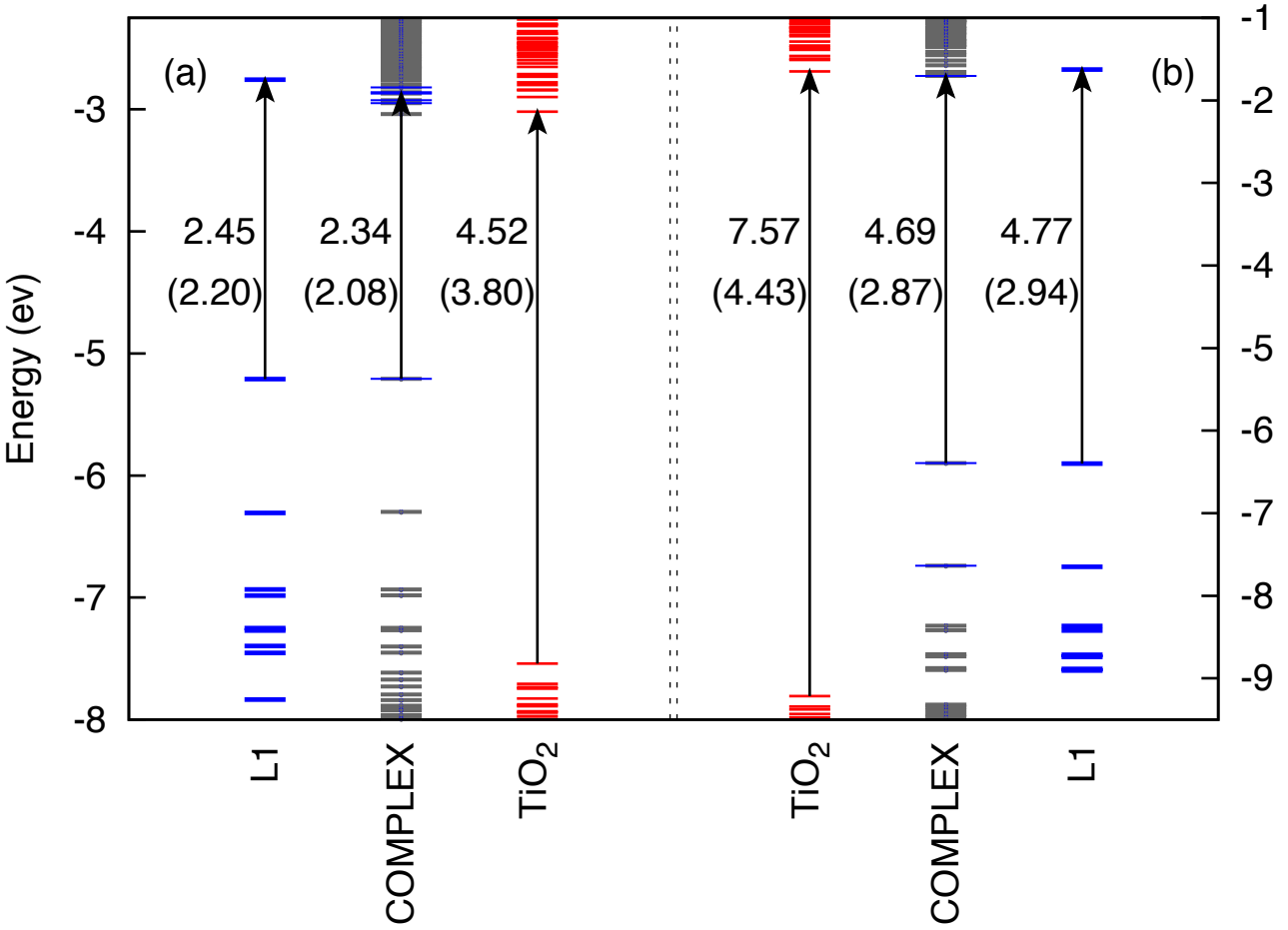
(a)
(b)
Energy (ev)
-3
-4
-5
-6
-7
-8
-1
-2
-3
-4
-5
-6
-7
-8
-9
2.45
(2.20)
2.34
(2.08)
4.52
(3.80)
7.57
(4.43)
4.69
(2.87)
4.77
(2.94)
L1
COMPLEX
TiO2
TiO2
COMPLEX
L1

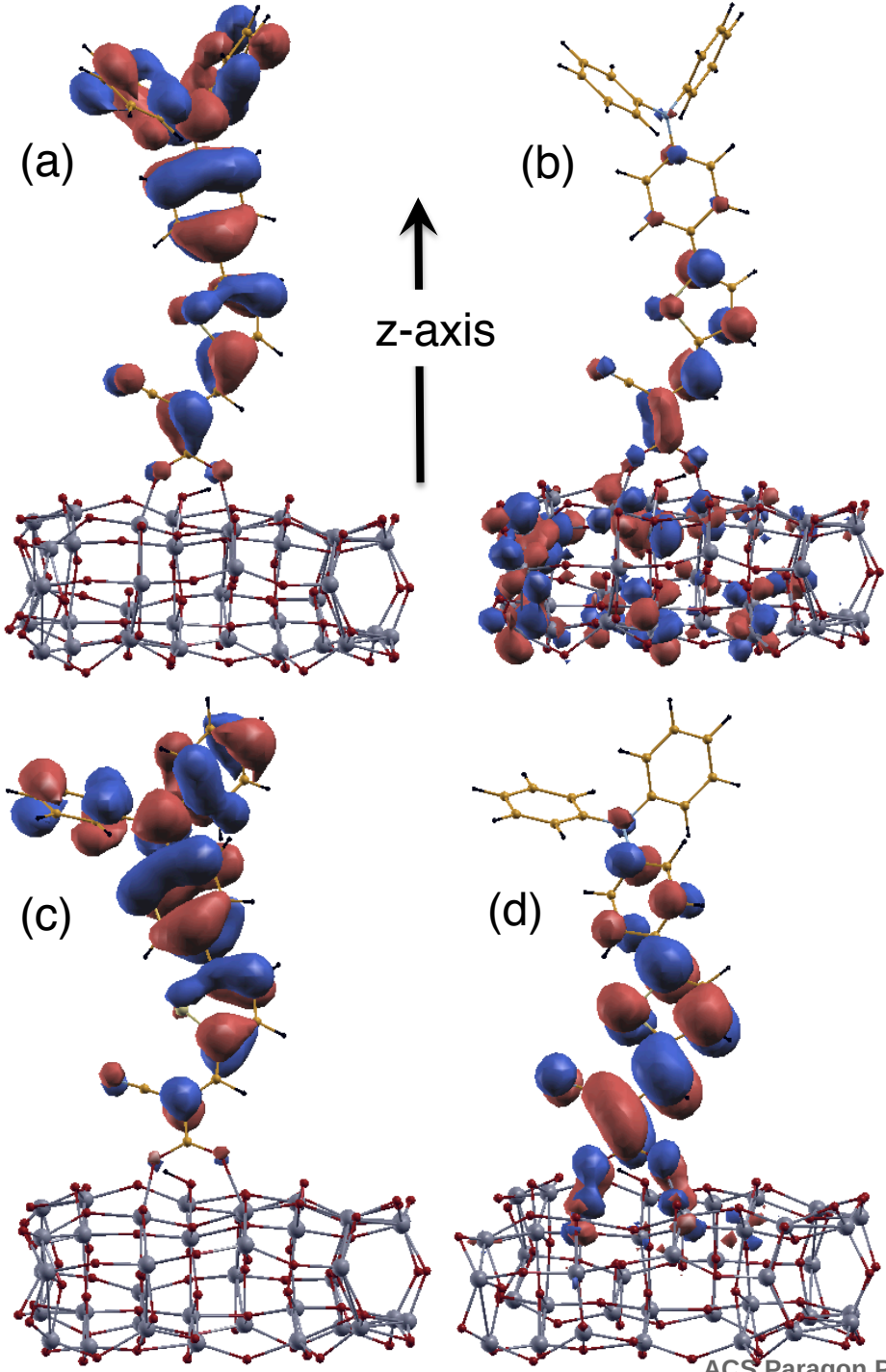
(a)
(b)
z-axis
(c)
(d)

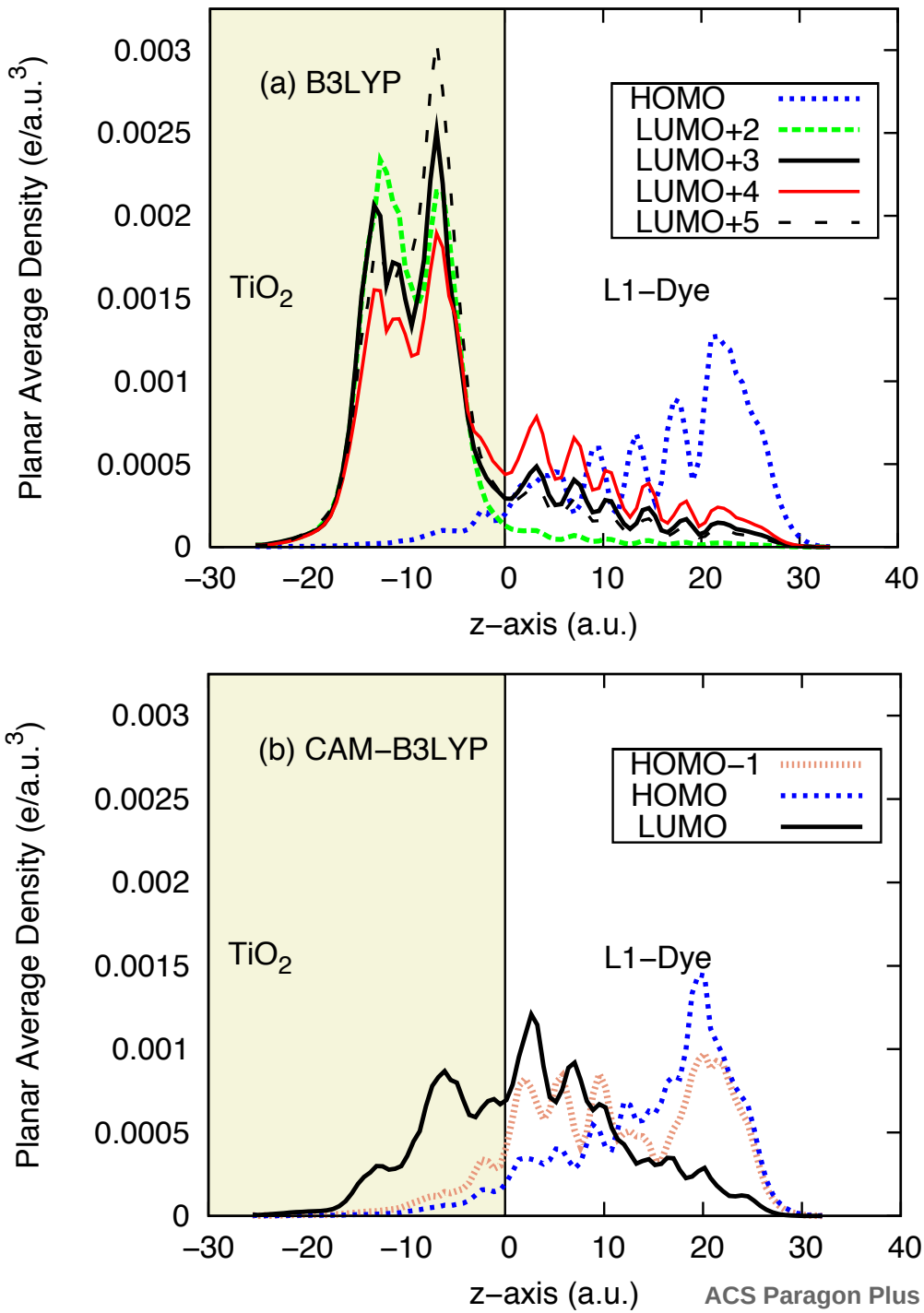

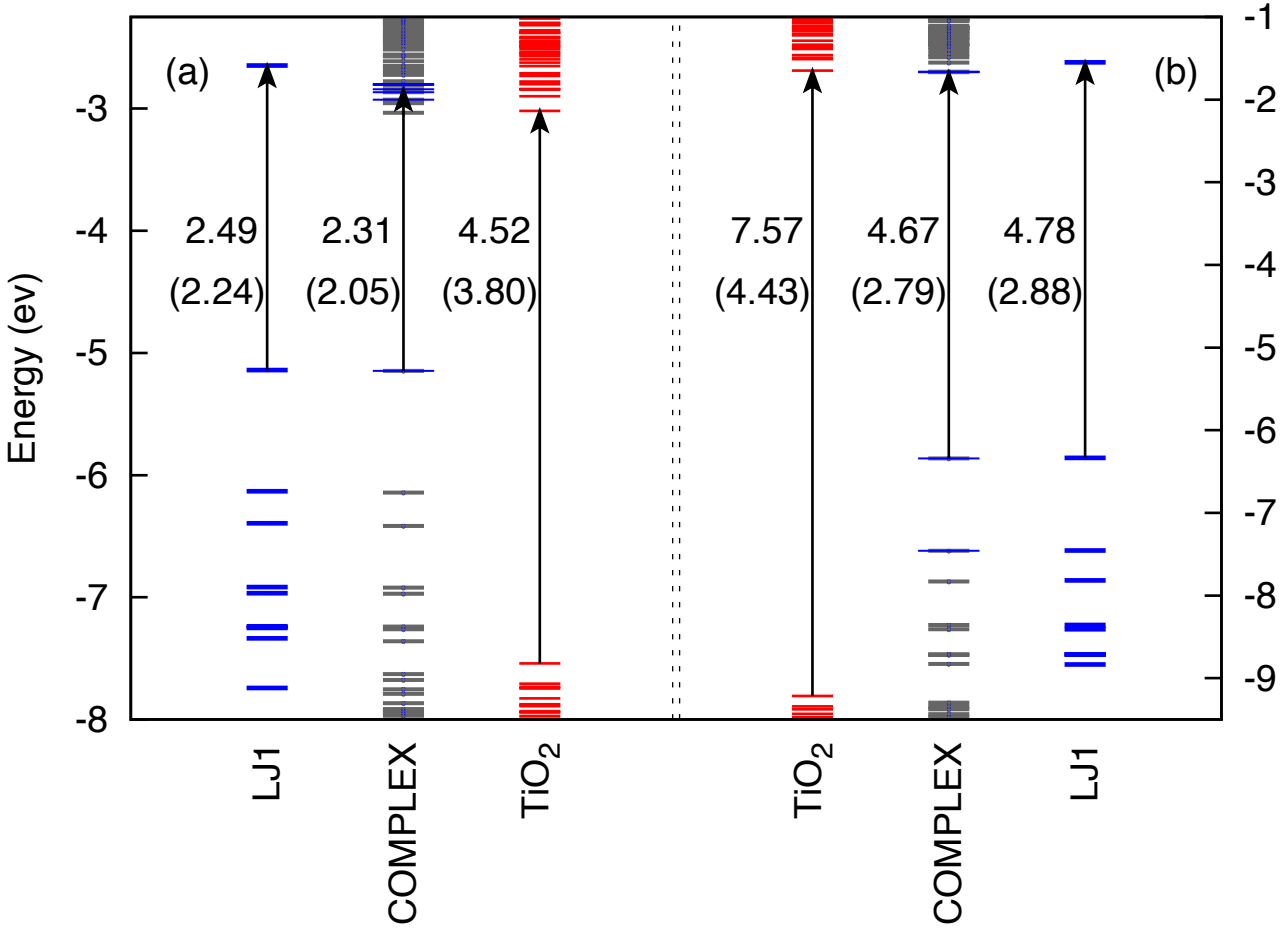
(a)
(b)
Energy (ev)
-1
-2
-3
-4
-5
-6
-7
-8
-9
2.49
(2.24)
2.31
(2.05)
4.52
(3.80)
7.57
(4.43)
4.67
(2.79)
4.78
(2.88)
LJ1
COMPLEX
TiO2
TiO2
COMPLEX
LJ1

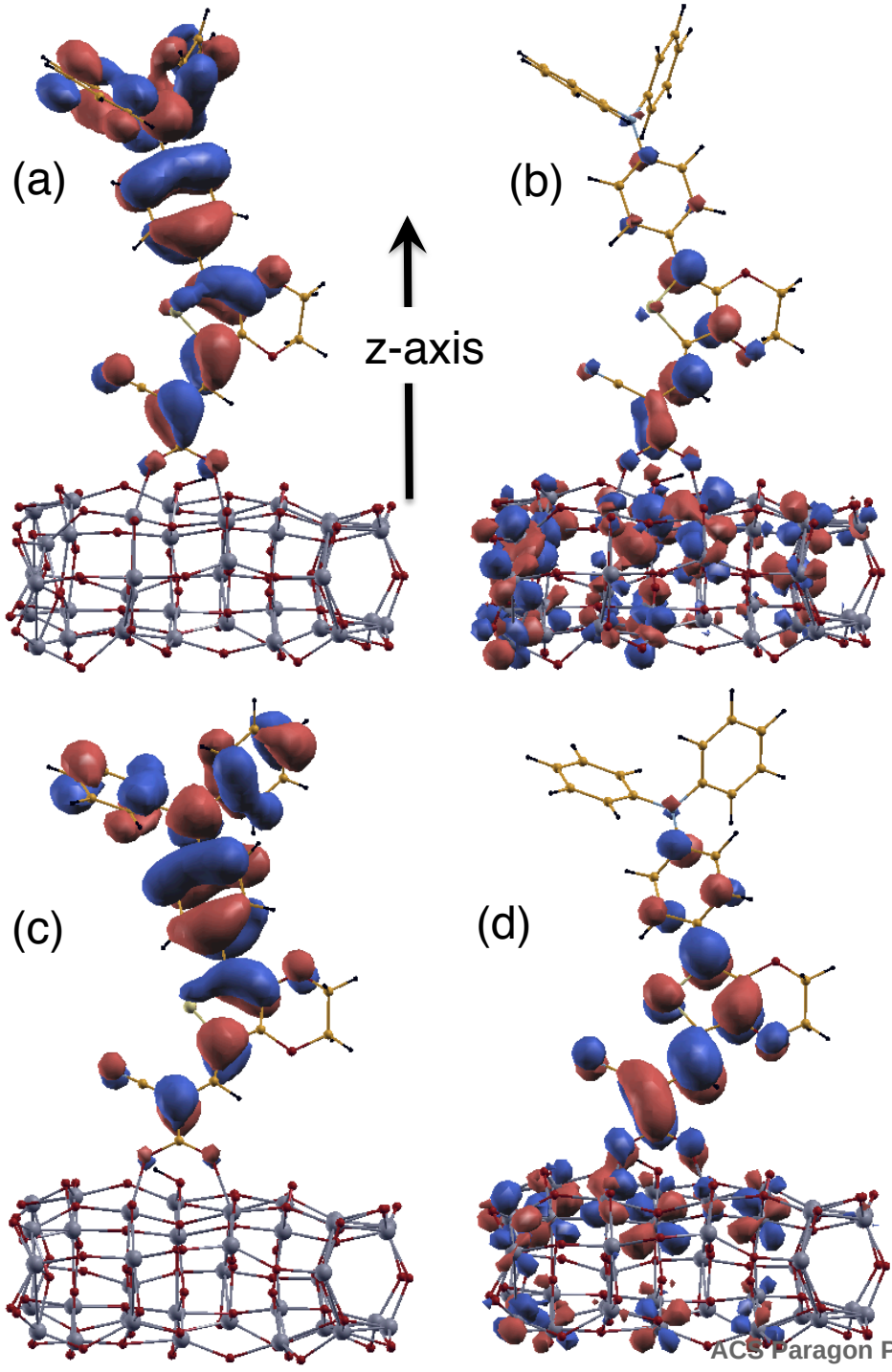

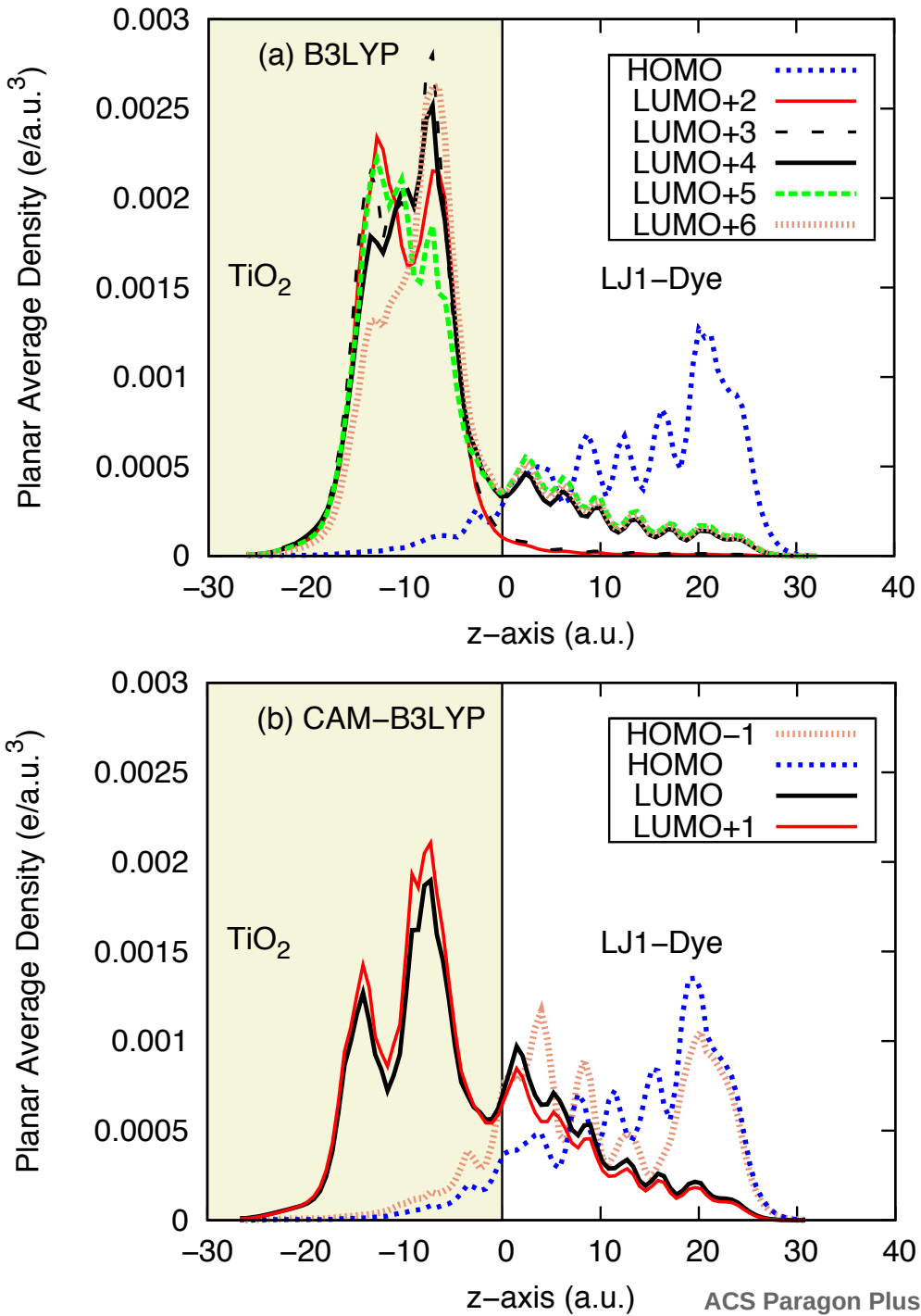

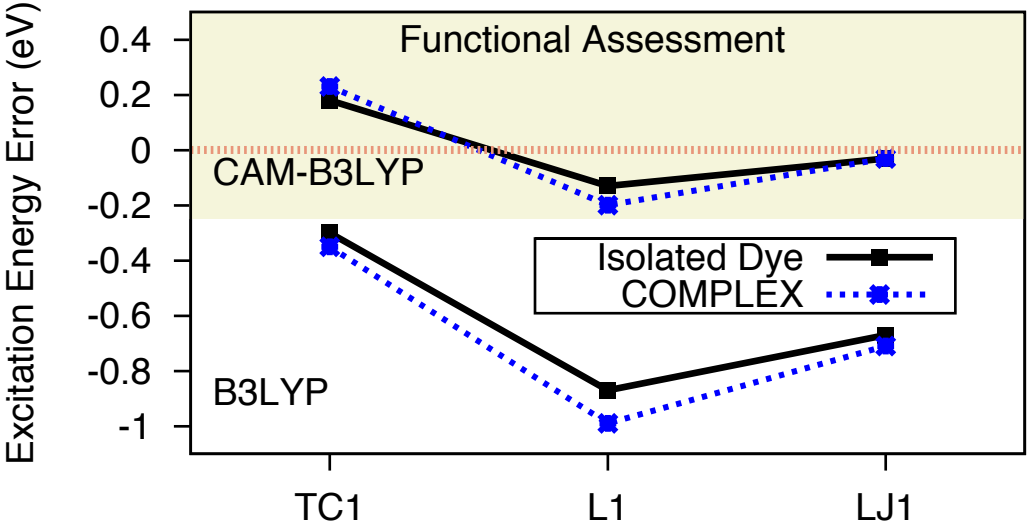
Functional Assessment
CAM-B3LYP
B3LYP
Isolated Dye
COMPLEX
Excitation Energy Error (eV)
0.4
0.2
0
-0.2
-0.4
-0.6
-0.8
-1
TC1
L1
LJ1